# Supplementary Information

## Evidential Deep Learning-based Drug-Target Interaction Prediction

Yanpeng Zhao [a, b †], Yuting Xing [c †], Yixin Zhang [a †], Yifei Wang [a], Mengxuan Wan [a, b], Duoyun Yi [a, d], Chengkun Wu [e, f], Shangze Li [a], Huiyan Xu [a, d], Hongyang Zhang [a, d], Ziyi Liu [a, c], Guowei Zhou [a, g], Mengfan Li [a], Xuanze Wang [a], Zhengshan Chen [a], Ruijiang Li [a], Lianlian Wu [a, g], Dongsheng Zhao [a], Peng Zan [d] *, Song He [a] *, Xiaochen Bo [a] *

a Academy of Military Medical Sciences, Beijing 100850, China

b School of Medicine, Shanghai University, Shanghai 200444, China

c Defense Innovation Institute, Academy of Military Science, Beijing 100071, China

d Shanghai Key Laboratory of Power Station Automation Technology, School of Mechatronics Engineering and Automation, Shanghai University, Shanghai 200444, China

e College of Computer Science and Technology, National University of Defense Technology, Changsha, 410000, Hunan, china

f Laboratory of Digitizing Software for Frontier Equipment, National University of Defense Technology, Changsha, 410000, Hunan, China

g Academy of Medical Engineering and Translational Medicine, Tianjin University, Tianjin 300072, China

* Corresponding authors.

E-mail addresses: boxc@bmi.ac.cn (Xiaochen Bo), hes1224@163.com (Song He), zanpeng@shu.edu.cn (Peng Zan)

† These authors contributed equally to this work.

# Supplementary Note 1

**Supplementary Table 1** Information of datasets used in the DTI prediction

| Datasets | Protein | Drug | Interaction | Positive | Negative |
|---|---|---|---|---|---|
| DrugBank | 4085 | 6148 | 33 062 | 16 531 | 16 531 |
| Davis | 379 | 68 | 25 772 | 7320 | 18 452 |
| KIBA | 225 | 2068 | 116 350 | 22 154 | 94 196 |

# Supplementary Results

**Supplementary Table 2** Comparison results of EviDTI and baselines on the cold start dataset.

| Cold start | Accuracy | Recall | Precision | MCC | F1 score | AUC | AUPR |
|---|---|---|---|---|---|---|---|
| DeepConv-DTI | 78.56 | 78.32 | 76.32 | 57.75 | 77.31 | 86.43 | 82.12 |
| GraphDTA | 76.23 | 74.76 | 75.34 | 52.54 | 75.05 | 84.23 | 82.54 |
| MolTrans | 78.70 | 78.59 | **86.64** | 57.37 | 78.05 | 85.87 | <u>86.64</u> |
| HyperAttention | 73.66 | <u>79.61</u> | 70.10 | 48.06 | 72.14 | 82.40 | 82.93 |
| TransformerCPI | 78.94 | 76.05 | 79.40 | 57.82 | 77.67 | **86.93** | **87.78** |
| GraphormerDTI | 76.16 | 68.88 | <u>80.87</u> | 53.19 | 74.14 | 83.15 | 85.27 |
| AIGO-DTI | 73.17 | 61.60 | 78.57 | 47.21 | 68.64 | 80.16 | 79.05 |
| DLM-DTI | <u>79.16</u> | 76.56 | 81.26 | <u>59.33</u> | <u>78.80</u> | 86.43 | 86.10 |
| EVIDTI | **79.96** | **81.20** | 78.09 | **59.97** | **79.61** | <u>86.69</u> | 85.43 |

Note: The best results are highlighted in bold, while the second-best results are underlined.

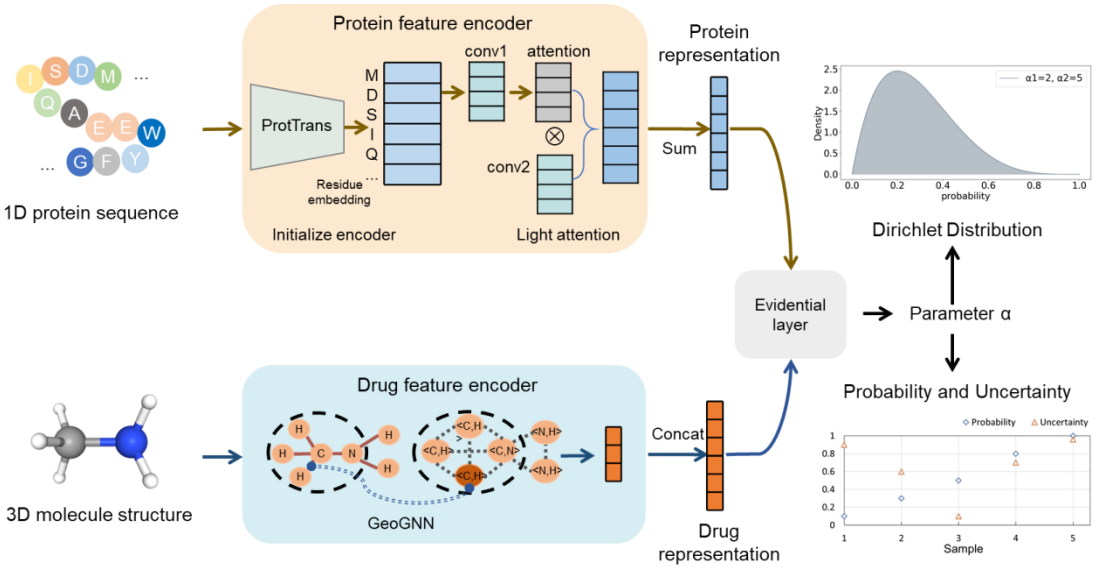


**Supplementary Figure 1 The flowchart of EviDTI w/o drug 2D.** Given a drug-target pair as input, the protein feature encoder utilizes the pre-trained model ProtTrans for initial target representation, further refined by a light attention (LA) module. The drug feature encoder learns the drug's 2D topology representations. For the 2D graph, the initial representation is derived from the pre-trained model MG-BERT and processed by a 1DCNN neural network. The target and drug representations are concatenated and fed into the evidence layer, which outputs parameter α to calculate prediction probability and corresponding uncertainty.

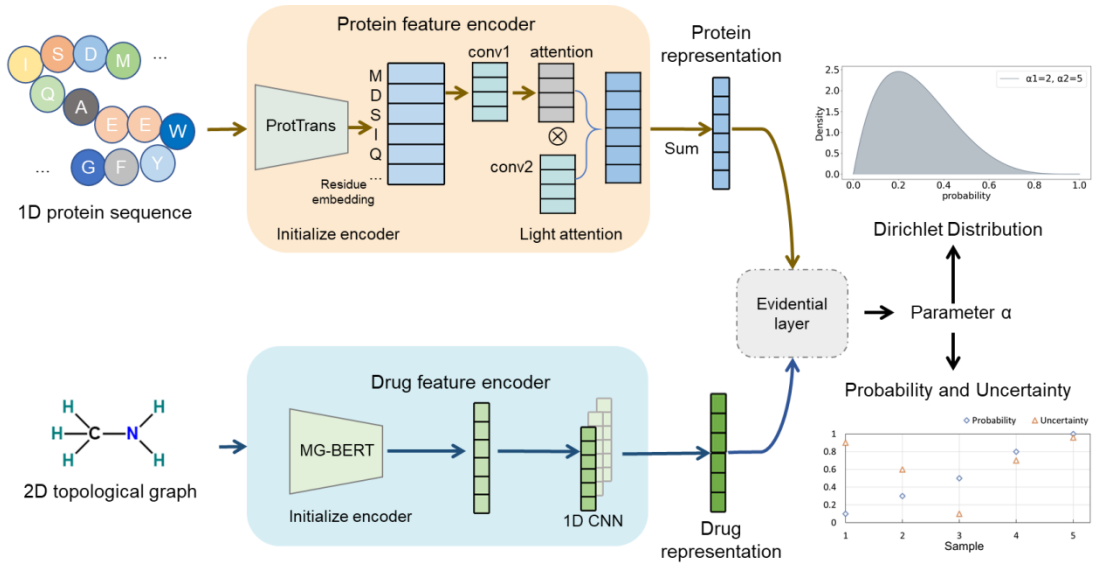


**Supplementary Figure 2 The flowchart of EviDTI w/o drug 3D.** Given a drug-target pair as input, the protein feature encoder utilizes the pre-trained model ProtTrans for initial target representation, further refined by a light attention (LA) module. The drug feature encoder learns the 3D structure representations. For the 3D structure, the representations were obtained via the GeoGNN module. The target and drug representations are concatenated and fed into the evidence layer, which outputs parameter α to calculate prediction probability and corresponding uncertainty.

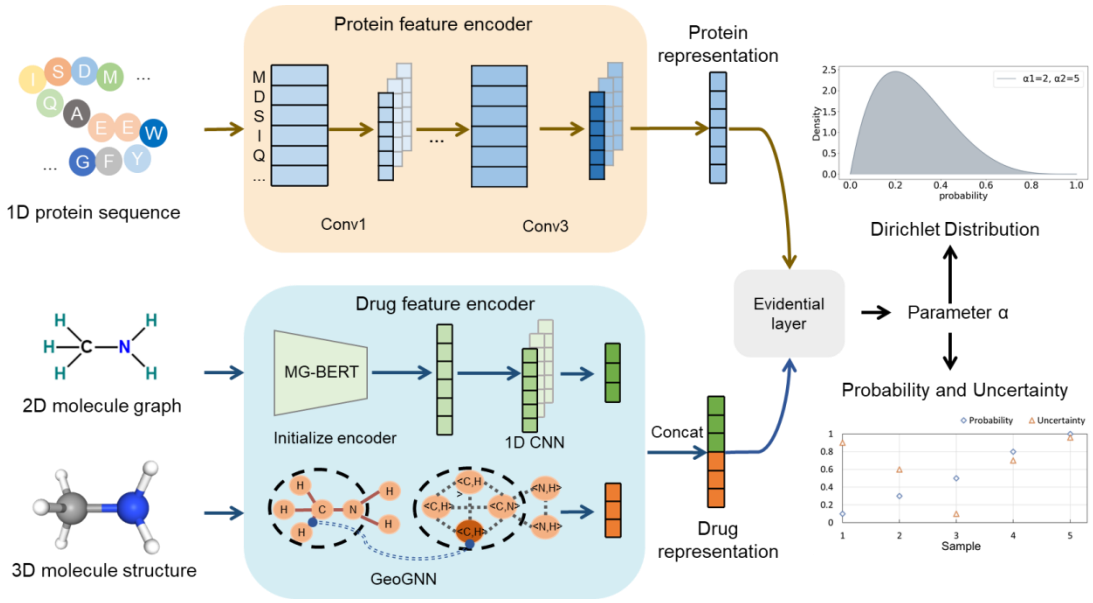


**Supplementary Figure 3 The flowchart of EviDTI-Protein Integer.** Given a drug-target pair as input, the protein feature encoder utilizes the integer coding and a CNN for feature extraction. The drug feature encoder learns the drug's 2D topology and 3D structure representations. For the 2D graph, the initial representation is derived from the pre-trained model MG-BERT and processed by a 1DCNN neural network. For the 3D structure, the representations were obtained via the GeoGNN module. The target and drug representations are concatenated and fed into the evidence layer, which outputs parameter α to calculate prediction probability and corresponding uncertainty.

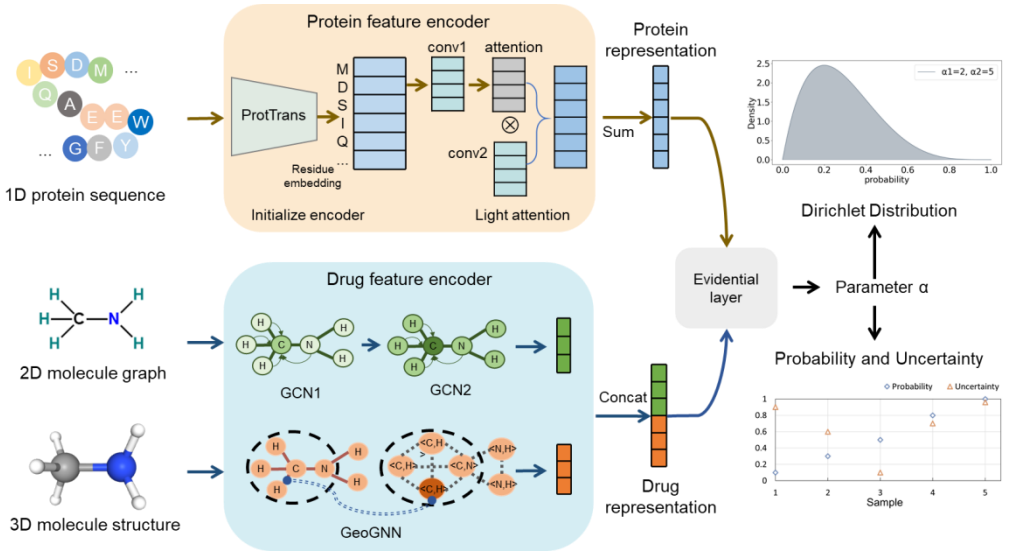


**Supplementary Figure 4 The flowchart of EviDTI-Drug 2D GCN.** Given a drug-target pair as input, the protein feature encoder utilizes the integer coding and a CNN for feature extraction. The drug feature encoder learns the drug's 2D topology and 3D structure representations. For the 2D graph, the molecule representation is learned via a two-layer GCN. For the 3D structure, the representations were obtained via the GeoGNN module. The target and drug representations are concatenated and fed into the evidence layer, which outputs parameter α to calculate prediction probability and corresponding uncertainty.

**Supplementary Table 3** Performance on the DrugBank, KIBA, Davis datasets with single-dimensional features and multidimensional feature fusion strategies

| Dataset | Strategies | Accuracy | Recall | Precision | MCC | F1 | AUC | AUPR |
|---|---|---|---|---|---|---|---|---|
| **DrugBank** | EviDTI | **82.02 (0.43)** | **82.28 (1.03)** | **81.90 (0.58)** | **64.29 (1.05)** | **82.09 (0.74)** | **88.87 (0.73)** | **88.45 (1.51)** |
| | EviDTI w/o drug 3D | 81.67 (0.54) | 80.90 (0.68) | 81.53 (0.83) | 63.42 (0.75) | 81.20 (0.73) | 88.04 (0.94) | 88.39 (0.97) |
| | EviDTI w/o drug 2D | 80.40 (0.94) | 81.27 (0.65) | 80.22 (0.65) | 60.75 (0.47) | 80.74 (0.65) | 86.95 (0.56) | 85.69 (0.45) |
| **KIBA** | EviDTI | **91.27 (0.07)** | **70.77 (1.69)** | **80.90 (1.32)** | **70.44 (0.78)** | **75.48 (0.83)** | **93.57 (0.35)** | **83.03 (0.98)** |
| | EviDTI w/o drug 3D | 90.99 (0.16) | 70.75 (0.76) | 78.53 (0.53) | 69.12 (0.57) | 74.43 (0.63) | 91.30 (0.32) | 81.73 (0.97) |
| | EviDTI w/o drug 2D | 90.35 (0.22) | 67.47 (0.90) | 78.02 (0.94) | 66.81 (1.00) | 72.36 (0.91) | 92.16 (0.46) | 80.40 (1.06) |
| **Davis** | EviDTI | **87.40 (1.08)** | 72.93 (1.93) | **81.17 (2.94)** | **68.40 (2.78)** | 76.81 (2.03) | **92.10 (0.78)** | **85.07 (2.12)** |
| | EviDTI w/o drug 3D | 87.15 (0.86) | **75.80 (1.13)** | 78.13 (2.71) | 67.85 (2.16) | **76.93 (1.63)** | 91.68 (0.36) | 84.11 (1.20) |
| | EviDTI w/o drug 2D | 87.02 (0.46) | 73.67 (1.55) | 79.10 (2.16) | 67.49 (1.25) | 76.26 (1.01) | 91.89 (0.63) | 84.33 (1.48) |

Note: The best results are highlighted in bold, while the second-best results are underlined. Five independent replications of each method were performed (n=5). Data are expressed as means (std).

**Supplementary Table 4** Performance on the DrugBank, KIBA, Davis datasets with the architectures that use pre-trained models for feature extraction and architectures that do not use pre-trained models

| Dataset | Architecture | Accuracy | Recall | Precision | MCC | F1 | AUC | AUPR |
|---|---|---|---|---|---|---|---|---|
| **DrugBank** | EviDTI | **82.02 (0.43)** | **82.28 (1.03)** | **81.90 (0.58)** | **64.29 (1.05)** | **82.09 (0.74)** | **88.87 (0.73)** | **88.45 (1.51)** |
| | EviDTI-Protein Integer | 80.90 (0.30) | 79.86 (1.23) | 81.79 (1.25) | 61.86 (0.45) | 80.80 (0.48) | 88.16 (0.21) | 88.03 (0.42) |
| | EviDTI-Drug 2D GCN | 73.27 (0.81) | 68.32 (3.72) | 75.87 (0.60) | 46.81 (1.40) | 71.84 (1.78) | 79.41 (1.45) | 79.29 (2.69) |
| **KIBA** | EviDTI | **91.27 (0.07)** | **70.77 (1.69)** | **80.90 (1.32)** | **70.44 (0.78)** | **75.48 (0.83)** | **93.57 (0.35)** | **83.03 (0.98)** |
| | EviDTI-Protein Integer | 90.95 (0.40) | 69.86 (1.36) | 78.91 (2.60) | 68.81 (1.14) | 74.07 (0.83) | 90.85 (0.46) | 81.62 (0.73) |
| | EviDTI-Drug 2D GCN | 90.42 (0.21) | 67.53 (1.44) | 78.65 (1.16) | 67.16 (0.33) | 72.65 (0.63) | 92.05 (0.33) | 80.54 (0.15) |
| **Davis** | EviDTI | **87.40 (1.08)** | 72.93 (1.93) | **81.17 (2.94)** | **68.40 (2.78)** | **76.81 (2.03)** | **92.10 (0.78)** | **85.07 (2.12)** |
| | EviDTI-Protein Integer | 85.54 (0.71) | 72.06 (1.37) | 75.70 (2.02) | 63.83 (1.90) | 73.83 (1.54) | 91.10 (0.51) | 83.01 (1.62) |
| | EviDTI-Drug 2D GCN | 87.01 (0.97) | 72.46 (1.34) | 79.84 (2.48) | 67.21 (2.31) | 75.96 (1.79) | 91.83 (0.45) | 84.58 (1.78) |

Note: The best results are highlighted in bold, while the second-best results are underlined. Five independent replications of each method were performed (n=5). Data are expressed as means (std).

**Supplementary Table 5** Comparison of OFR between evidential-based framework and probability-based framework on DrugBank, KIBA and Davis dataset at different thresholds

| Dataset | framework | OFR | | | | | | | | | |
|---|---|---|---|---|---|---|---|---|---|---|---|
| | | **0.1** | **0.09** | **0.08** | **0.07** | **0.06** | **0.05** | **0.04** | **0.03** | **0.02** | **0.01** |
| **DrugBank** | uncertainty | 15.01 | 14.72 | 14.38 | 14.05 | 13.54 | 12.72 | 11.20 | 9.28 | 7.64 | 4.78 |
| | | (0.6) | (0.6) | (0.7) | (0.7) | (0.5) | (0.1) | (0.3) | (0.3) | (0.2) | (0.6) |
| | probability | 11.20 | 11.07 | 10.83 | 10.64 | 10.19 | 10.09 | 9.92 | 9.26 | 8.88 | 7.59 |
| | | (3.5) | (3.4) | (3.5) | (3.5) | (3.1) | (2.7) | (2.7) | (2.7) | (2.4) | (2.5) |
| **KIBA** | uncertainty | 5.02 | 4.72 | 4.37 | 4.08 | 3.71 | 3.36 | 2.95 | 2.33 | 1.58 | 0.78 |
| | | (0.5) | (0.5) | (0.5) | (0.5) | (0.4) | (0.4) | (0.5) | (0.4) | (0.2) | (0.2) |
| | probability | 3.28 | 3.16 | 2.98 | 2.81 | 2.66 | 2.49 | 2.26 | 1.96 | 1.72 | 1.42 |
| | | (0.7) | (0.6) | (0.5) | (0.5) | (0.5) | (0.4) | (0.4) | (0.4) | (0.3) | (0.2) |
| **Davis** | uncertainty | 7.35 | 7.03 | 6.59 | 6.16 | 5.53 | 4.78 | 3.74 | 2.75 | 1.95 | 0.80 |
| | | (0.4) | (0.5) | (0.4) | (0.4) | (0.4) | (0.6) | (0.5) | (0.8) | (0.9) | (0.6) |
| | probability | 5.58 | 5.28 | 5.07 | 4.78 | 4.46 | 3.97 | 3.50 | 3.17 | 2.60 | 2.15 |
| | | (0.1) | (0.1) | (0.2) | (0.3) | (0.4) | (0.3) | (0.3) | (0.2) | (0.4) | (0.3) |

Note: Five independent replications of each method were performed (n=5). Data are expressed as means (std).

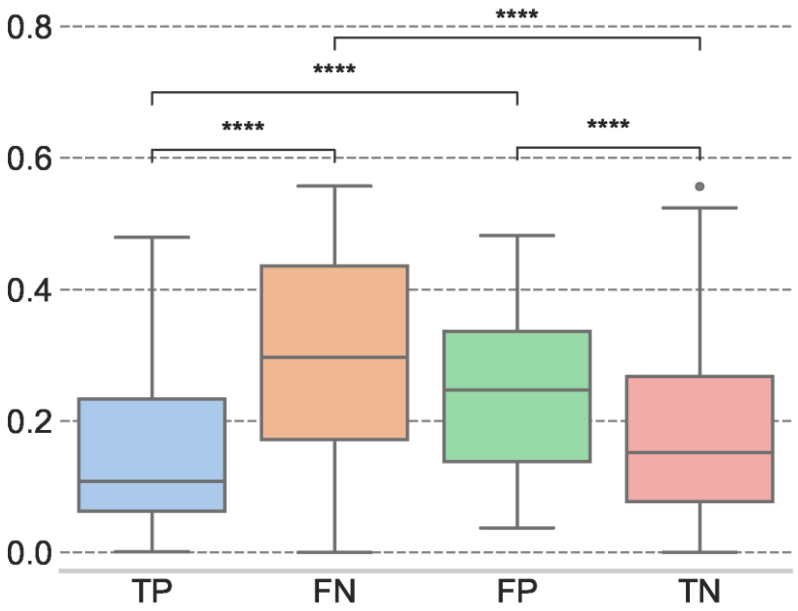


**Supplementary Figure 5** The Mann-Whitney test was performed on the cold-start dataset (n=3173) on the distribution of uncertainty errors for samples categorized as TP, FP, FN, TN. The central line indicates the median, the box bounds indicate the 25th and 75th percentiles, whiskers extend to the minimum and maximum values (within 1.5× interquartile range), and outliers are shown as individual points. All tests were two-sided, with no adjustments made for multiple comparisons. Asterisks indicate statistically significant differences based on Mann-Whitney U test p-values: ****$p \leq 0.0001$. Significance is indicated as follows: For cold-start dataset, TP vs. FN has a p-value of 1.694e-44, FP vs. TN has a p-value of 1.585e-15, TP vs. FP has a p-value of 3.180e-36, FN vs. TN has a p-value of 1.046e-25. Source data are provided as a Source Data file.

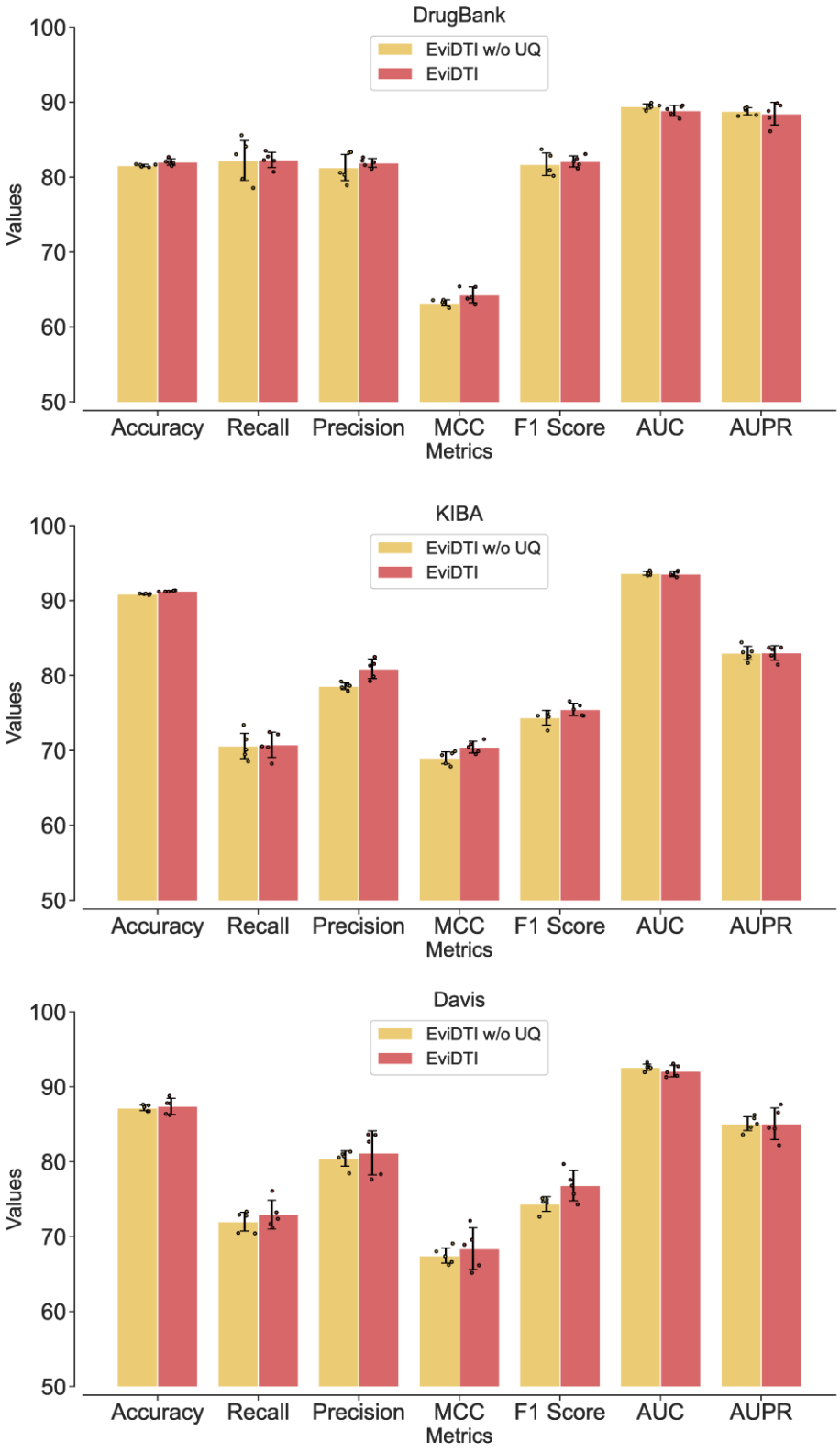


**Supplementary Figure 6** Performance comparison on the DrugBank, KIBA and Davis datasets using uncertainty quantification and using non-uncertainty quantification strategies. Five independent replications of each method were performed (n=5). Data are expressed as means ± std. Source data are provided as a Source Data file.

**Supplementary Table 6 Prediction of two levatinib analogues from open patents on 11 potential targets using EviDTI**

| Drug patent ID | Target name | Uniport id | Rank | PRED | TRUE |
|---|---|---|---|---|---|
| LYD-2-45 | FGFR2 | P21802 | 1 | 1 | 1 |
| | FGFR1 | P11362 | 2 | 1 | 1 |
| | FLT4 | P35916 | 3 | 1 | 1 |
| | KIT | P10721 | 4 | 1 | 1 |
| | MET | P08581 | 5 | 1 | 0 |
| | REY | P07949 | 6 | 1 | 1 |
| | EGFR | P00533 | 7 | 1 | 0 |
| | PDGFβ | P01127 | 8 | 0 | 1 |
| | FLT1 | P17948 | 9 | 1 | 1 |
| | FGFR3 | P22607 | 10 | 1 | 1 |
| | PDGFα | P16234 | 11 | 1 | 1 |
| LYD-2-49 | KIT | P10721 | 1 | 1 | 1 |
| | FLT4 | P35916 | 2 | 1 | 1 |
| | FLT1 | P17948 | 3 | 1 | 1 |
| | EGFR | P00533 | 4 | 1 | 0 |
| | RET | P07949 | 5 | 1 | 1 |
| | FGFR1 | P11362 | 6 | 1 | 1 |
| | FGFR2 | P21802 | 7 | 1 | 1 |
| | MET | P08581 | 8 | 1 | 0 |
| | FGFR3 | P22607 | 9 | 1 | 1 |
| | PDGFβ | P01127 | 10 | 0 | 1 |
| | PDGFα | P16234 | 11 | 1 | 1 |

**Supplementary Table 7** Top 10 predicted interactions with the lowest uncertainty between tyrosine kinase modulators and tyrosine kinase targets

| Compound | Target | Rank | Probability (Uncertainty) | Consistency with literature |
|---|---|---|---|---|
| RG 14620 | SRC | 1 | 98.37 (0.0327) | - |
| Tyrphostin 9 | KIT/ SCFR | 2 | 98.14 (0.0373) | - |
| GSK180736A | KIT/ SCFR | 3 | 98.08 (0.0384) | - |
| NS309 | SRC | 4 | 98.03 (0.0393) | - |
| Tolimidone | SRC | 5 | 97.94 (0.0412) | - |
| **Flumatinib mesylate** | **c-Kit** | **6** | **97.91 (0.0419)** | Zhao, J. *et al.*[1] |
| BIX02188 | KIT/ SCFR | 7 | 97.90 (0.0421) | - |
| Tyrphostin 9 | VEGFR3 | 8 | 97.89 (0.0421) | - |
| GSK180736A | FLT3 | 9 | 97.85 (0.0429) | - |
| **Flumatinib mesylate** | **Bcr-Abl** | **10** | **97.85 (0.0429)** | Zhao, J. *et al.*[1] |

**Supplementary Table 8** Predicted probabilities and uncertainties of literature-reported DTIs between tyrosine kinase modulators and tyrosine kinase targets

| Compound | Target | Probability | Uncertainty | Predicted results | Reference |
|---|---|---|---|---|---|
| Flumatinib mesylate | c-Kit | 97.91 | 0.0419 | 1 | Zhao, J. *et al.*[1] |
| Flumatinib mesylate | Bcr-Abl | 97.85 | 0.0429 | 1 | Zhao, J. *et al.*[1] |
| 5'-Fluoroindirubinoxime | FLT3 | 97.70 | 0.0461 | 1 | Choi, S. J. *et al.*[2] |
| MNS | Src | 97.46 | 0.0508 | 1 | Wang *et al.*[3] |
| SB1317 hydrochloride | FLT3 | 97.39 | 0.0523 | 1 | William, A. D. *et al.*[4] |
| Tyrphostin 9 | PDGFR | 96.29 | 0.0742 | 1 | Kandandapani, S. *et al.*[5] |
| Edicotinib | CSF-1R | 96.16 | 0.0769 | 1 | Mancuso, R. *et al.*[6] |
| Edicotinib | FLT3 | 95.74 | 0.0852 | 1 | Genovese, M. C. *et al.*[7] |
| XL228 | Lyn | 95.37 | 0.0926 | 1 | Clary, D. O. *et al.* [8] |
| Ilginatinib maleate | JAK2 | 95.25 | 0.0949 | 1 | Nakaya, Y. *et al.*[9] |
| MNS | Syk | 94.12 | 0.1176 | 1 | Wang *et al.*[3] |
| SB1317 hydrochloride | JAK2 | 94.11 | 0.1178 | 1 | William, A. D. *et al.*[4] |
| SSR128129E | FGFR | 93.71 | 0.1258 | 1 | Bono, F. *et al.*[10] |
| MCB613 | SRC | 93.66 | 0.1268 | 1 | Wang, L. *et al.*[11] |
| Su1498 | VEGFR2 | 93.14 | 0.1372 | 1 | Boguslawski, G. *et al.*[12] |
| (E/Z)-Zotiraciclib | JAK2 | 93.12 | 0.1375 | 1 | Khalid Pasha *et al.*[13] |
| Flumatinib mesylate | PDGFRβ | 92.29 | 0.1541 | 1 | Zhao, J. *et al.* [1] |
| FLLL32 | JAK2 | 89.75 | 0.2049 | 1 | Bill, M. A. *et al.*[14] |
| (E/Z)-Zotiraciclib | FLT3 | 89.10 | 0.2181 | 1 | Khalid Pasha. *et al.*[13] |
| MNS | FAK | 83.61 | 0.3278 | 1 | Wang *et al.*[3] |
| Degrasyn | JAK2 | 74.90 | 0.5019 | 1 | Bartholomeusz. *et al.*[15] |
| Tyrphostin AG 879 | TrKA | 7.29 | 0.1457 | 0 | Levitzki, A. *et al.*[16] |
| Tolimidone | Lyn | 5.73 | 0.1145 | 0 | Saporito, M. S. *et al.*[17] |
| AG1024 | IGF-1R | 3.13 | 0.0627 | 0 | Párrizas, M. *et al.*[18] |
| Tanshinone IIA | VEGFR2 | 2.93 | 0.0585 | 0 | Xie, J. *et al.*[19] |
| ZM 39923 HCl | JAK3 | 2.64 | 0.0528 | 0 | Zhang, Z. *et al.*[20] |
| Pralsetinib | RET | 1.17 | 0.0233 | 0 | Subbiah, V. *et al.*[21] |

Note: A predicted result of 1 indicates that the model considers the drug and target to interact, while a predicted result of 0 indicates that the model considers the drug and target to have no interaction.

**Supplementary Table 9** Predicted probabilities and uncertainties of interactions between drugs in the top 10 DTIs and their literature-reported targets

| Compound | Targets reported in the literature | Probability (Uncertainty) | Predicted results |
|---|---|---|---|
| RG 14620 | EGFR[22] | 96.52 (0.0696) | 1 |
| Tyrphostin 9 | PDGFR[5] | 96.29 (0.0741) | 1 |
| GSK180736A | GRK[23] | 2.08 (0.0415) | 0 |
| | ROCK1[24] | 89.19 (0.2163) | 1 |
| NS309 | Potassium Channel[25] | 93.89(0.1222) | 1 |
| Tolimidone | LYN[26] | 5.73 (0.1145) | 0 |
| Flumatinib mesylate | c-Kit[1] | 97.91 (0.0419) | 1 |
| | Bcr-Abl[1] | 97.85 (0.0429) | 1 |
| | PDGFR[1] | 92.29 (0.1541) | 1 |
| BIX02188 | MEK5[27] | 12.26 (0.0245) | 0 |

Note: A predicted result of 1 indicates that the model considers the drug and target to interact, while a predicted result of 0 indicates that the model considers the drug and target to have no interaction.

**Supplementary Table 10a** The 50% effective concentration of compounds with the lowest uncertainty against FAK

| Compound | FAK | | | |
|---|---|---|---|---|
| | Rank | Probability (Uncertainty) | The 50% effective concentration (nM)[a] | The molecule's effect on FAK |
| Tyrphostin 9 | 1 | 97.69 (0.0461) | 35.7±3.4 | inhibitor |
| GSK180736A | 2 | 97.65 (0.0469) | >10000 | - |
| Vodobatinib | 7 | 97.04 (0.0591) | 85.7 ± 8.2 | inhibitor |
| BIX02188 | 3 | 97.58 (0.0484) | >10000 | - |
| PKG drug G1 | 5 | 97.22 (0.0555) | >10000 | - |
| ST 271 | 4 | 97.31 (0.0537) | >10000 | - |
| Flumatinib | 6 | 97.18 (0.0564) | 14.9 ± 2.1 | inhibitor |

[a] Values are the means of three replicates

**Supplementary Table 10b** The 50% effective concentration of compounds with the lowest uncertainty against FLT3

| Compound | FLT3 | | | |
|---|---|---|---|---|
| | Rank | Probability (Uncertainty) | The 50% effective concentration (nM)[a] | The molecule's effect on FLT3 |
| Tyrphostin 9 | 1 | 97.90 (0.0419) | 1265.9±244.6 | activator |
| GSK180736A | 2 | 97.85 (0.0429) | >10000 | - |
| Vodobatinib | 3 | 97.69 (0.0461) | 406.8±74.5 | activator |
| BIX02188 | 4 | 97.60 (0.0480) | >10000 | - |
| PKG drug G1 | 5 | 97.60 (0.0481) | >10000 | - |
| ST 271 | 6 | 97.53 (0.0494) | >10000 | - |
| Flumatinib | 9 | 97.13 (0.0573) | >10000 | - |

[a] Values are the means of three replicates

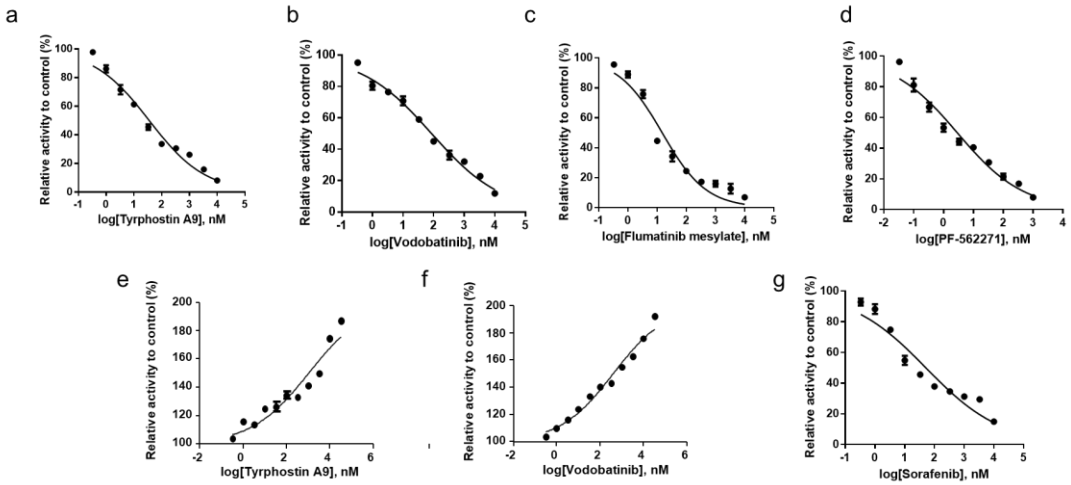


**Supplementary Figure 7 a-d** Concentration-activity curves of Tyrphostin 9, Vodobatinib, Flumatinib and PF-562271 in the FAK kinase ADP-Glo assays, respectively. PF-562271 as positive control. Mean ± SEM of three independent experiments is shown (n=3). **e-g** Concentration-activity curves of Vodobatinib, Tyrphostin 9 and sorafenib in the FLT3 kinase ADP-Glo assays, respectively. Sorafenib as positive control. Mean ± SEM of three independent experiments is shown (n=3).

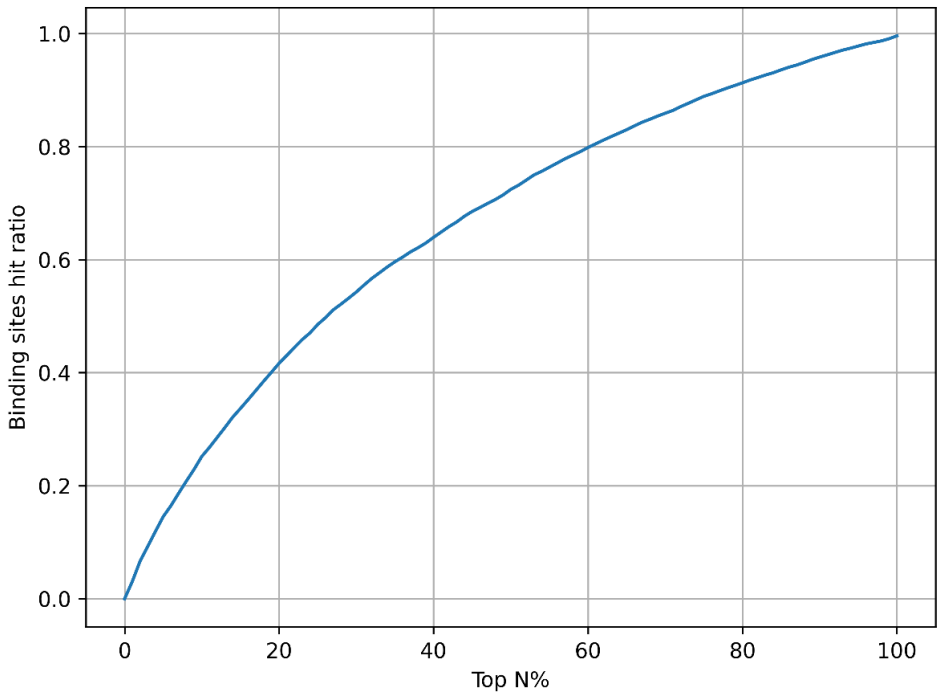


**Supplementary Fig 8** Binding sites hit ratio of residues with higher attention to the binding site at different thresholds

# Supplementary Methods

**a) Evaluation metrics**

First, a few relevant definitions are introduced:

TP (True-Positive) represents the number of samples that are actually positive cases and are determined as positive cases by the classifier.

FP (False-Positive) represents the number of samples that are actually negative cases but are determined as positive cases by the classifier.

FN (False-Negative) represents the number of samples that are actually positive cases but are determined as negative cases by the classifier.

TN (True-Negative) represents the number of samples that are actually negative cases and are determined as negative cases by the classifier.

**Accuracy**

Accuracy represents the ratio between the correctly predicted samples and the total samples:

$$\text{Accuracy} = \frac{\text{TP} + \text{TN}}{\text{TP} + \text{FP} + \text{TN} + \text{FN}} \tag{1}$$

**Precision**

Precision is an important evaluation metric, especially in binary classification problems, that measures the accuracy of positive predictions made by a model. It's a measure of how many of the instances predicted as positive are actually positive.

$$\text{Precision} = \frac{\text{TP}}{\text{TP} + \text{FP}} \tag{2}$$

**Recall**

Recall, also known as sensitivity or true positive rate, is an important evaluation metric in classification that measures the ability of a model to correctly identify all positive instances.

$$\text{Recall} = \frac{\text{TP}}{\text{TP} + \text{FN}} \tag{3}$$

**F1 score**

The macro algorithm calculates Precision and Recall by first calculating Precision and Recall for each category and then taking the average.

$$\text{F1} = 2 \cdot \frac{\text{precision} \cdot \text{recall}}{\text{precision} + \text{recall}} \tag{4}$$

**AUC**

The evaluation indicator AUC stands for Area Under the Curve. The curve refers to the Receiver Operating Characteristic (ROC) curve, which plots the true positive rate (sensitivity) against the false positive rate (1 - specificity) for various classification thresholds.

**Sensitivity** (also known as recall or true positive rate): Sensitivity measures the proportion of actual positive instances correctly identified by the model.

$$\text{Sensitivity} = \frac{\text{TP}}{\text{TP} + \text{FN}} \tag{5}$$

**Specificity**: Specificity measures the proportion of actual negative instances correctly identified by the model.

$$\text{Specificity} = \frac{\text{TN}}{\text{TN} + \text{FP}} \tag{6}$$

The AUC value ranges from 0 to 1, where a higher value indicates better performance. A perfect classifier would have an AUC of 1, while a random or ineffective classifier would have an AUC close to 0.5.

**AUPR**

The evaluation indicator AUPR stands for Area Under the Precision-Recall Curve. It is an evaluation metric used to assess the performance of classification models, particularly in scenarios where imbalanced class distribution is present or when the focus is on the positive class.

Unlike AUC, which is based on the Receiver Operating Characteristic (ROC) curve, AUPR is based on the Precision-Recall curve. The Precision-Recall curve plots the precision (positive predictive value) against the recall (sensitivity) for different classification thresholds.

The AUPR value ranges from 0 to 1, with a higher value indicating better performance. A perfect classifier would have an AUPR of 1, while a random or ineffective classifier would have an AUPR close to the proportion of positive instances in the dataset.

**OFR**

To examine whether Evidential DTI can reduce the percentage of false high-confidence predictions relative to traditional classification models, we defined "high confidence predictions" as samples with $p^i > 1 - T$ or $p^i < T$, where T is a threshold between 0-0.1. The "overconfidence false sample rate" (OFR) was further defined as the percentage of samples with high confidence forecasts for which $p^i > 1 - T$ and $y^i = 0$ or $p^i < T$ and $y^i = 1$:

$$\text{OFR} = \frac{\sum_i 1\left(\left(p^i > 1 - T \text{ and } y^i = 0\right) \text{ or } \left(p^i < T \text{ and } y^i = 1\right)\right)}{\sum_i 1\left(\left(p^i > 1 - T\right) \text{ or } \left(p^i < T\right)\right)} \tag{7}$$

## b) Training details

## Hyperparameter optimization

**Supplementary Table 11 Hyperparameter of Evidential DTI**

| Parameter | Range |
|---|---|
| Epoch | 500 |
| batch | 32 |
| optim | adam |
| learning rate | 5e-4 |
| weight_decay | 1.0e-5 |
| dropout | 0.3 |
| Target feature convolution kernel size | 9 |
| Target attention convolution kernel size | 9 |
| Target readout MLP layers | 1 |
| Target readout MLP hidden dimension | 256 |
| Drug 2D feature convolution layers | 2 |
| Drug 2D feature convolution kernel size | 3 |
| Drug 2D readout MLP layers | 2 |
| Drug 2D readout MLP hidden dimension | [1024,128] |
| Drug 3D GNN model | [GAT, GNNTransformer] |
| Drug 3D GNN layers | [4, 6, 8] |
| heads | [1, 4] |
| Drug 3D GNN embed dim | 64 |
| Drug 3D readout MLP layers | 2 |
| Drug 3D readout MLP hidden dimension | [1024, 128] |
| DTI readout MLP layers | 4 |
| DTI readout MLP hidden dimension | [1024,1024,512,2] |
| Final activation | softplus |

## Impact of hyperparameter

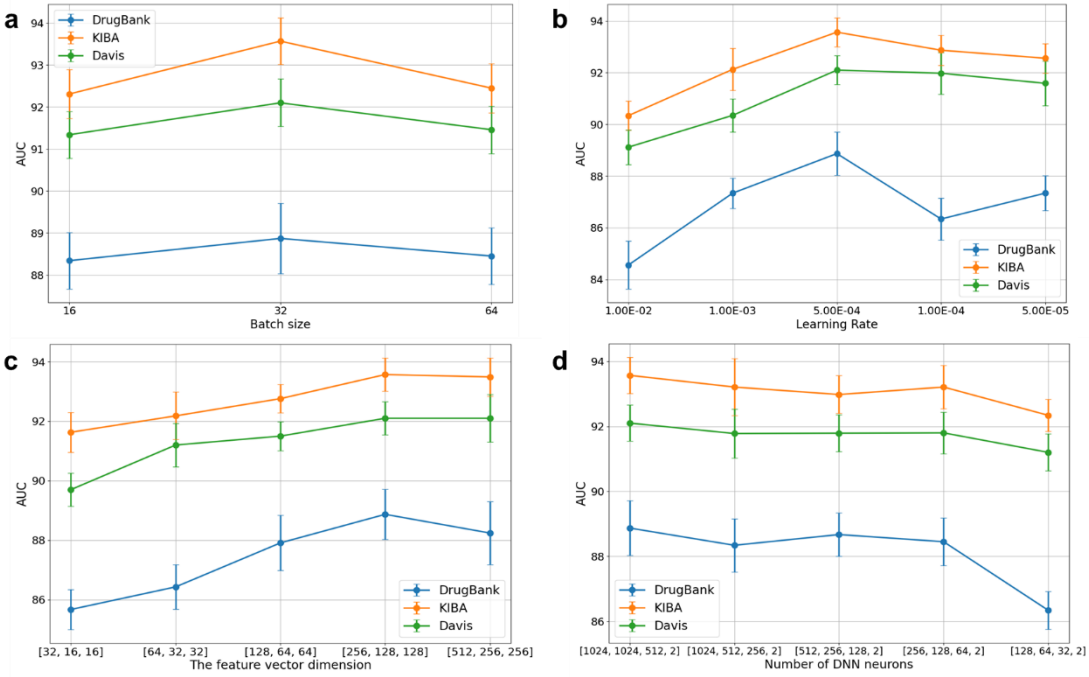


**Supplementary Figure 9** Impact of hyperparameter on AUC. Five independent replications of each experimental were performed (n=5). Data are expressed as means (std).

For the key hyperparameters of each major component (e.g., learning rate, batch size, hidden layer dimension, etc.), we adopted a grid search approach to explore different hyperparameter combinations. Specifically: we first determined the impact of different learning rates and batch sizes on the results through a series of preliminary experiments. These experiments helped us find the optimal combination of learning rate and batch size that would accelerate convergence while avoiding overfitting. Next, we explored the effect of different feature dimensions of the target (protein) and drug on the model performance. The aim of this phase was to find the optimal dimensionality settings that adequately capture the features of the input data without leading to an overly complex model structure. Based on the base configuration identified in the above step, we further explored the effect of the number of neurons in the fully connected layer on model performance. This step aims to balance model complexity with predictive power to ensure that the model not only performs well on the training set, but also maintains good generalization ability on the validation and test sets. As shown in Fig. S8, the final selected hyperparameter combination performs well on several performance metrics (e.g., accuracy, precision, MCC, AUC), which further proves its

223 effectiveness and general applicability.
224

## Supplementary References:


1. Zhao, J. *et al.* Flumatinib, a selective inhibitor of BCR-ABL/PDGFR/KIT, effectively overcomes drug resistance of certain KIT mutants. *Cancer Science* **105**, 117–125 (2014).
2. Choi, S. J. *et al.* Indirubin derivatives as potent FLT3 inhibitors with anti-proliferative activity of acute myeloid leukemic cells. *Bioorganic & Medicinal Chemistry Letters* **20**, 2033–2037 (2010).
3. Wang, W.-Y., Wu, Y.-C. & Wu, C.-C. Prevention of Platelet Glycoprotein IIb/IIIa Activation by 3,4-Methylenedioxy-β-Nitrostyrene, A Novel Tyrosine Kinase Inhibitor. *Molecular Pharmacology* **70**, 1380–1389 (2006).
4. William, A. D. *et al.* Discovery of kinase spectrum selective macrocycle (16E)-14-methyl-20-oxa-5,7,14,26-tetraazatetracyclo[19.3.1.1(2,6).1(8,12)]heptacosa-1(25),2(26),3,5,8(27),9,11,16,21,23-decaene (SB1317/TG02), a potent inhibitor of cyclin dependent kinases (CDKs), Janus kinase 2 (JAK2), and fms-like tyrosine kinase-3 (FLT3) for the treatment of cancer. *J Med Chem* **55**, 169–196 (2012).
5. Kandandapani, S., Ridzwan ,Nor Farrah Wahidah, Mohamad ,Saharuddin B. & and Tayyab, S. Exploring the interaction between tyrphostin 9 and human serum albumin using biophysical and computational methods. *Journal of Biomolecular Structure and Dynamics* **38**, 4134–4142 (2020).
6. Mancuso, R. *et al.* CSF1R inhibitor JNJ-40346527 attenuates microglial proliferation and neurodegeneration in P301S mice. *Brain* **142**, 3243–3264 (2019).
7. Genovese, M. C. *et al.* Results from a Phase IIA Parallel Group Study of JNJ-40346527, an Oral CSF-1R Inhibitor, in Patients with Active Rheumatoid Arthritis despite Disease-modifying Antirheumatic Drug Therapy. *J Rheumatol* **42**, 1752 (2015).

8. Clary, D. O. *et al.* Abstract C192: Characterization of the target profile of XL228, a multi-targeted protein kinase inhibitor in phase 1 clinical development. *Molecular Cancer Therapeutics* **8**, C192–C192 (2009).

9. Nakaya, Y. *et al.* Efficacy of NS-018, a potent and selective JAK2/Src inhibitor, in primary cells and mouse models of myeloproliferative neoplasms. *Blood Cancer Journal* **1**, e29–e29 (2011).

10. Bono, F. *et al.* Inhibition of Tumor Angiogenesis and Growth by a Small-Molecule Multi-FGF Receptor Blocker with Allosteric Properties. *Cancer Cell* **23**, 477–488 (2013).

11. Wang, L. *et al.* Characterization of a Steroid Receptor Coactivator Small Molecule Stimulator that Overstimulates Cancer Cells and Leads to Cell Stress and Death. *Cancer Cell* **28**, 240–252 (2015).

12. Boguslawski, G., McGlynn, P. W., Harvey, K. A. & Kovala, A. T. SU1498, an Inhibitor of Vascular Endothelial Growth Factor Receptor 2, Causes Accumulation of Phosphorylated ERK Kinases and Inhibits Their Activity in Vivo and in Vitro*. *Journal of Biological Chemistry* **279**, 5716–5724 (2004).

13. Khalid Pasha, M. *et al.* Preclinical Metabolism and Pharmacokinetics of SB1317 (TG02), a Potent CDK/JAK2/FLT3 Inhibitor. *Drug Metabolism Letters* **6**, 33–42 (2012).

14. Bill, M. A. *et al.* The small molecule curcumin analog FLLL32 induces apoptosis in melanoma cells via STAT3 inhibition and retains the cellular response to cytokines with anti-tumor activity. *Molecular Cancer* **9**, 165 (2010).

15. Bartholomeusz, G. A., Donato, N., Estrov, Z., Priebe, W. & Talpaz, M. Activation of a Novel Proteasomal Independent Bcr/Abl Degradation Pathway by WP1130 Induces Apoptosis in CML Cells. *Blood* **106**, 2862–2862 (2005).

16. Levitzki, A. & Gazit, A. Tyrosine Kinase Inhibition: An Approach to Drug Development. *Science* **267**, 1782–1788 (1995).

17. Saporito, M. S., Ochman, A. R., Lipinski, C. A., Handler, J. A. & Reaume, A. G. MLR-1023 Is a Potent and Selective Allosteric Activator of Lyn Kinase In Vitro That Improves Glucose Tolerance In Vivo. *The Journal of Pharmacology and Experimental Therapeutics* **342**, 15–22 (2012).

18. Párrizas, M., Gazit, A., Levitzki, A., Wertheimer, E. & LeRoith, D. Specific Inhibition of Insulin-Like Growth Factor-1 and Insulin Receptor Tyrosine Kinase Activity and Biological Function by Tyrphostins. *Endocrinology* **138**, 1427–1433 (1997).

19. Xie, J. *et al.* The antitumor effect of tanshinone IIA on anti-proliferation and decreasing VEGF/VEGFR2 expression on the human non-small cell lung cancer A549 cell line. *Acta Pharmaceutica Sinica B* **5**, 554–563 (2015).

20. Zhang, Z. *et al.* Jak3 is involved in CCR7-dependent migration and invasion in metastatic squamous cell carcinoma of the head and neck Corrigendum in /10.3892/ol.2024.14712. *Oncol Lett* **13**, 3191–3197 (2017).

21. Subbiah, V. *et al.* Precision Targeted Therapy with BLU-667 for RET-Driven Cancers. *Cancer Discovery* **8**, 836–849 (2018).

22. Yoneda, T. *et al.* The Antiproliferative Effects of Tyrosine Kinase Inhibitors Tyrphostins on a Human Squamous Cell Carcinoma in Vitro and in Nude Mice1. *Cancer Research* **51**, 4430–4435 (1991).

23. Inagaki, S. *et al.* G Protein-Coupled Receptor Kinase 2 (GRK2) and 5 (GRK5) Exhibit Selective Phosphorylation of the Neurotensin Receptor in Vitro. *Biochemistry* **54**, 4320–4329 (2015).

24. Homan, K. T. *et al.* Identification and Structure–Function Analysis of Subfamily Selective G Protein-Coupled Receptor Kinase Inhibitors. *ACS Chem. Biol.* **10**, 310–319 (2015).

25. Stankevičius, E. *et al.* Opening of Small and Intermediate Calcium-Activated Potassium Channels Induces Relaxation Mainly Mediated by Nitric-Oxide Release in Large Arteries and Endothelium-Derived Hyperpolarizing Factor in Small Arteries from Rat. *The Journal of Pharmacology and Experimental Therapeutics* **339**, 842–850 (2011).

26. Saporito, M. S., Ochman, A. R., Lipinski, C. A., Handler, J. A. & Reaume, A. G. MLR-1023 Is a Potent and Selective Allosteric Activator of Lyn Kinase In Vitro That Improves Glucose Tolerance In Vivo. *The Journal of Pharmacology and Experimental Therapeutics* **342**, 15–22 (2012).

27. Tatake, R. J. *et al.* Identification of pharmacological inhibitors of the MEK5/ERK5 pathway. *Biochemical and Biophysical Research Communications* **377**, 120–125 (2008).